V.A.3 Drive-Cycle Performance of Automotive Fuel Cell Systems

Rajesh K. Ahluwalia (Primary Contact),
Xiaohua Wang, Romesh Kumar
Argonne National Laboratory
9700 South Cass Avenue
Argonne, IL 60439
Phone: (630) 252-5979
E-mail: walia@anl.gov

DOE Manager
HQ: Nancy Garland
Phone: (202) 586-5673
E-mail: Nancy.Garland@ee.doe.gov

Project Start Date: October 1, 2003
Project End Date: Project continuation and direction determined annually by DOE

Fiscal Year (FY) 2011 Objectives

- Develop a validated model for automotive fuel cell systems, and use it to assess the status of the technology.
- Conduct studies to improve performance and packaging, to reduce cost, and to identify key research and development (R&D) issues.
- Compare and assess alternative configurations and systems for transportation and stationary applications.
- Support DOE/U.S. DRIVE automotive fuel cell development efforts.

Technical Barriers

This project addresses the following technical barriers from the Fuel Cells section of the Fuel Cell Technologies Program Multi-Year Research, Development and Demonstration Plan:

(B) Cost
(C) Performance
(E) System Thermal and Water Management
(F) Air Management
(G) Startup and Shutdown Time and Energy/Transient Operation

Technical Targets

This project is conducting system level analyses to address the following DOE 2015 technical targets for automotive fuel cell power systems operating on direct hydrogen:

- Energy efficiency: 50%-60% (55%-65% for the stack) at 100%-25% of rated power.
- Power density: 650 W/L for system, 2,000 W/L for the stack.
- Specific power: 650 W/kg for system, 2,000 W/kg for the stack.
- Transient response: 1 s from 10% to 90% of rated power.
- Start-up time: 30 s from –20°C and 5 s from +20°C ambient temperature.
- Precious metal content: 0.2 g/kW.

FY 2011 Accomplishments

- Determined the performance of nanostructured thin film catalyst (NSTFC) stacks at low temperatures and on drive cycles.
- Evaluated the dynamic performance of the Honeywell integrated compressor-expander-motor (CEM) module.
- Analyzed the dynamic performance of a parallel ejector-pump hybrid for fuel management.
- Analyzed the dynamic performance of planar and supported liquid membrane humidifiers.
- Analyzed the dynamic performance of microchannel automotive radiators and polymer electrolyte fuel cell (PEFC) stacks during cold start on drive cycles.
- Conducted drive-cycle simulations to determine the fuel economy of hybrid fuel cell vehicles, ownership cost, and optimum fuel cell system (FCS) operating parameters.

Introduction

While different developers are addressing improvements in individual components and subsystems in automotive fuel cell propulsion systems (i.e., cells, stacks, balance-of-plant components), we are using modeling and analysis to address issues of thermal and water management, design-point and part-load operation, and component-, system-, and vehicle-level efficiencies and fuel economies. Such analyses are essential for effective system integration.

Approach

Two sets of models are being developed. The GCtool software is a stand-alone code with capabilities for design, off-design, steady-state, transient, and constrained optimization analyses of FCSs. A companion code, GCtool-ENG, has an alternative set of models with a built-in procedure for translation to the MATLAB®/Simulink® platform commonly used in vehicle simulation codes, such as Autonomie.

Results

In FY 2011, we analyzed the dynamic performance of an 80-kW_e net automotive FCS, shown in Figure 1, and its major components (fuel cell stack, and air, fuel, water and thermal management subsystems) on drive cycle transients [1]. The reference FCS is designed to achieve 45% efficiency at rated power (on the lower heating value basis). The stack operates at 75°C and 1.5-atm inlet pressure, the hydrogen and oxygen utilizations are 50%, and the cell voltage is 622 mV. The dew point temperatures at stack inlet are 61°C for cathode air and 53°C for hydrogen after mixing with the recirculated spent anode gas. Here, the stack temperature refers to the coolant exit temperature, the anode and cathode streams flow in opposite directions (counterflow), and the coolant flows in the same direction as the cathode air (coflow) with a 10°C temperature rise across the stack at rated power.

Figure 1 shows the in-line sensors (thermocouples, pressure transducer, differential pressure transducer, voltmeter, ammeter, and shaft revolutions per minute, rpm) used in our model to control and respond to the dynamic loads. The control model is based on a simple hierarchical logic that does not depend on measuring flow rates. The starting step is to determine the resistive load to vary the cell current, using the measured stack voltage as the guide. The control of the air management system is based on knowing the compressor discharge pressure and the shaft rotating speed (rpm). The model determines the direct current (DC) power to be applied to the motor controller and adjusts the turbine nozzle area as the power demand changes. The fuel management system relies on the measured differential pressure between the cathode and anode inlets to regulate the hydrogen flow rate. The control variable for the water management system is the flow rate of the low-temperature coolant (LTC) to the air pre-cooler using the LTC temperature at the outlet of the traction motor as the measurable temperature. Separate but similar controls are used for the high-temperature coolant (HTC) and LTC circuits of the thermal management system. The control of the HTC circuit depends on the measured HTC temperature at the stack outlet, and the control of the LTC circuit is based on the measured temperature of the LTC at the outlet of the traction motor.

Performance of the Air Management Subsystem

We used experimental data obtained on a full-scale, 100 $g.s^{-1}$ dry air, unit to model Honeywell's CEM with a variable nozzle turbine (VNT) [2-4]. The component maps were incorporated into a model for the compressor,

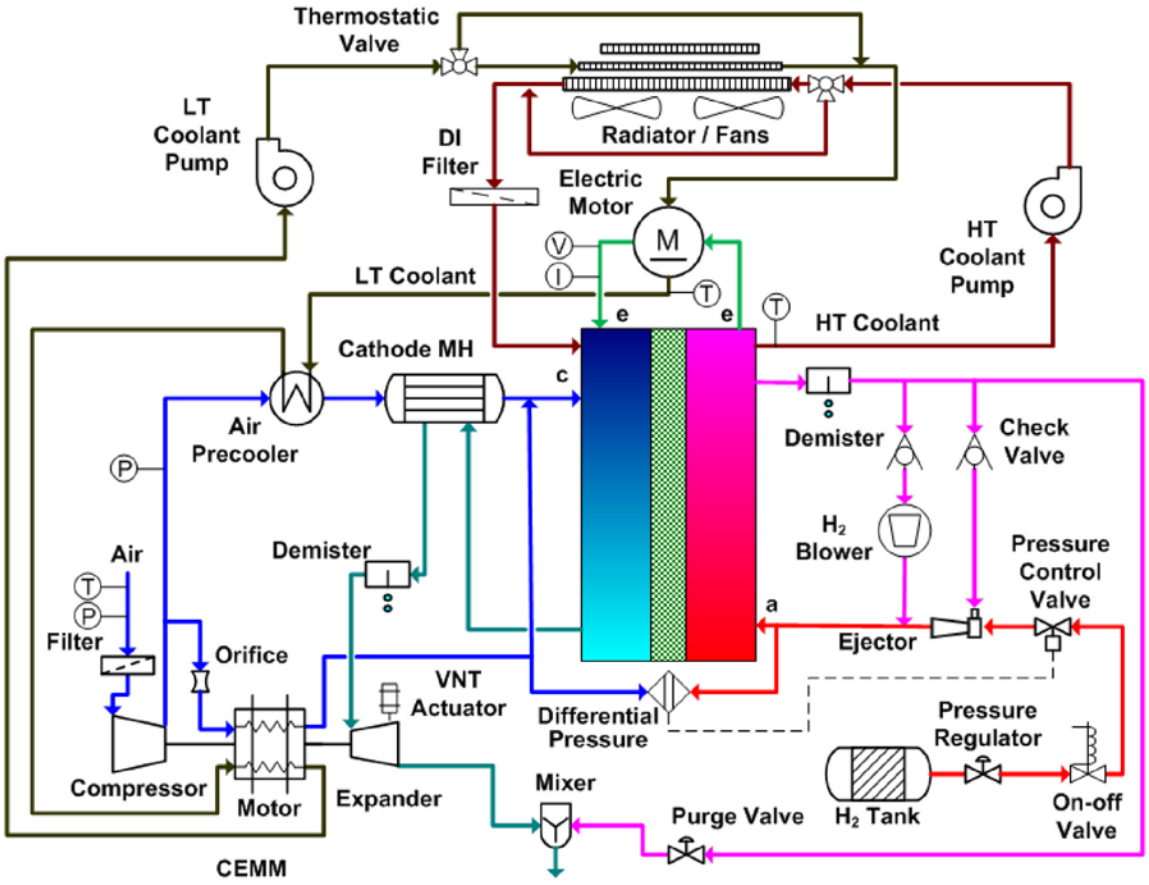

FIGURE 1. Reference FCS with In-line Sensors

expander, and motor that are mounted on a common shaft. The shaft is supported on airfoil bearings, and the motor is powered through a motor controller (DC input). This model was used to analyze the performance of two CEM configurations, one with and one without an expander. The model showed that recovering the compressor bleed air that cools the motor (configuration b with 1-psi pressure drop) reduces the CEM parasitic power by 0.4 to 1.6 kW. Also, an expander reduces the parasitic power by 4 kW if the stack inlet pressure is 2.5 atm (referred to as system S1), and by 1.5 kW if the stack inlet pressure is 1.5 atm (designated as system S2). We found that the CEM turndown (ratio of maximum to minimum flow rate) is a function of the minimum shaft speed (rpm) and may be limited by the compressor surge line. It is desirable to have turndown >10 and a minimum rpm <35,000; otherwise the CEM parasitic power at idle can be >500 W. The minimum shaft speed, if lower than the airfoil bearing lift speed of 36,000 rpm, will affect the durability of the airfoil bearings.

We conducted dynamic simulations to analyze the performance of the CEM (0.25 kg.m^2 moment of inertia) on urban (UDDS) and highway (HWFET) drive cycles [3]. We first developed a map for the optimum shaft speed and nozzle area as a function of the air flow rate (FCS power) at steady state; the map also specified the compressor discharge pressure and the CEM parasitic power at part load. We used the map as the reference to determine the target CEM operating conditions for the dynamic simulations. Given a particular power demand, the nozzle area was adjusted to the target value (assuming that the VNT actuator is fast acting), and the DC power to be applied to the motor controller to reach the target rpm in 100 ms was determined. We assumed that the motor in the CEM could be overloaded to 150% of the design value (6 kW for system S2) for short durations.

The symbols in Figure 2a represent the electric power that must be supplied to the CEM on the UDDS and HWFET drive cycles in the S2 system with an expander and configuration (b). These may be compared with the solid line that represents the power consumed by the CEM at steady state. We see that the power consumed by the CEM during an acceleration transient can be substantially greater than

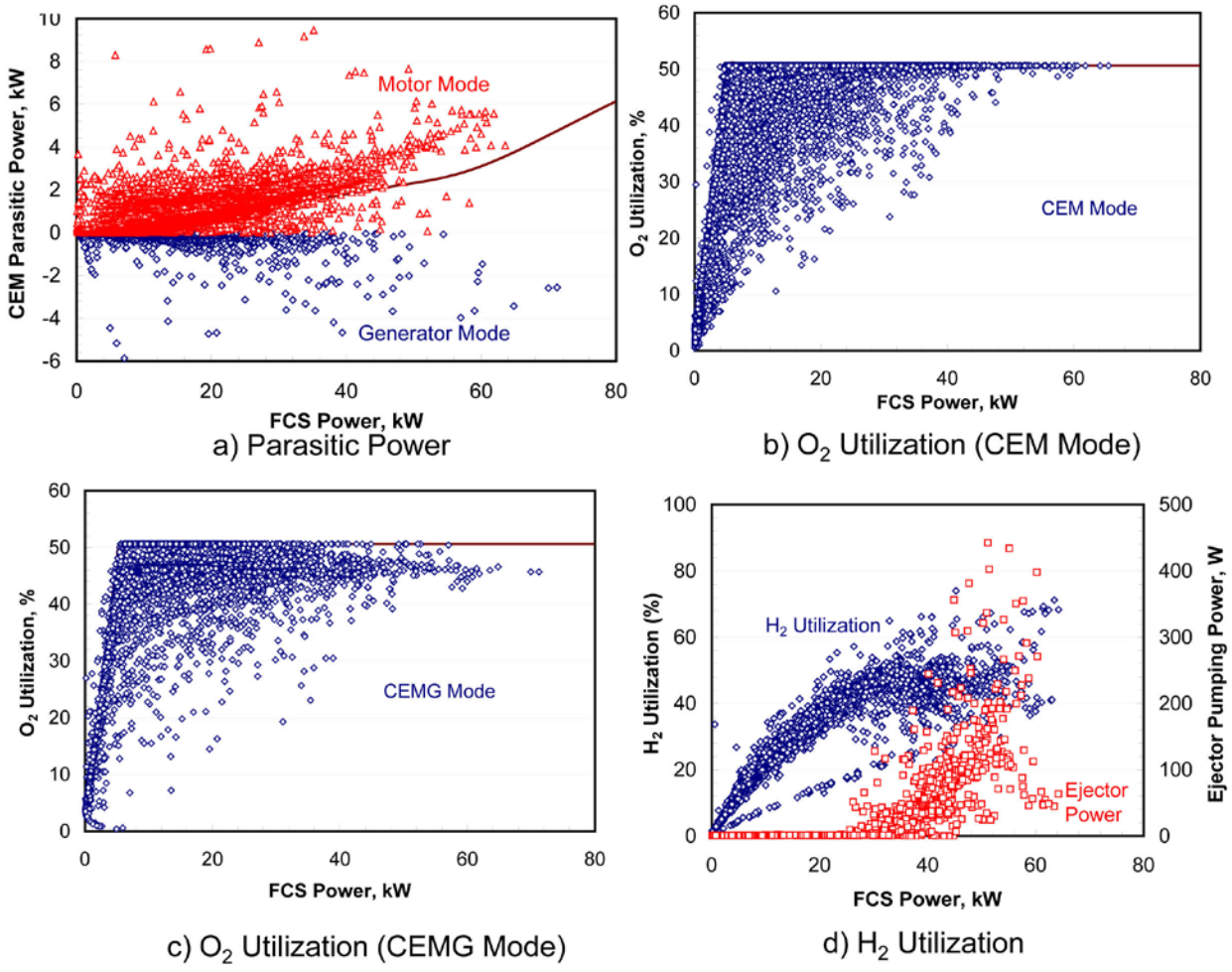

(symbols: dynamic results; solid line: steady-state simulation)

FIGURE 2. Dynamic Performance of the Air and Fuel Management Subsystems

the power required at steady state because of the extra power needed to increase the shaft speed. Conversely, the power consumed by the CEM during a deceleration transient can be less than the power required at steady-state conditions and may even be zero. Similarly, Figure 2b compares the oxygen utilization on the UDDS and HWFET cycles with the steady-state values represented as solid lines for 50% O_2 utilization and a maximum turndown of 20. We see that the cathode stoichiometric ratio (reciprocal of oxygen utilization) is >2 during deceleration and >>5 at low FCS power.

We also conducted simulations to assess the benefits of operating the motor as a compressor expander motor-generator module (CEMG). Figure 2a shows instances where there is net production of power by the CEMG unit during hard deceleration. However, the instances of higher than steady-state CEMG power requirement are also more frequent, since the shaft speed decreases faster during deceleration and must be increased more rapidly during a subsequent acceleration. Figure 2c indicates that the scattered data points are clustered closer to the steady-state O_2 utilization curve because of faster response to the deceleration transients.

Performance of the Fuel Management Subsystem

We developed a model to analyze the performance of a parallel ejector-pump hybrid in the fuel management system [3]. We considered that the motive gas is pure hydrogen from the compressed gas tank and the suction gas is spent hydrogen from the stack outlet. We assumed that the motive gas is available at a pressure no less than 22 bar (regarded as the empty tank pressure) and that the suction gas is saturated with water vapor (molecular weight of 3-7) at 1-1.15 atm (S2 scenario).

Our dynamic control algorithm for the fuel management system consists of a pressure regulator to lower the pressure of motive hydrogen to 22 bar and a pressure control valve to further lower the pressure at the inlet to the ejector. The hydrogen flow rate is varied by changing the pressure at the throat of the ejector in order to have zero differential pressure across the cathode and anode channels. The maximum hydrogen flow rate is set to 150% of the value at rated power.

Figure 2d summarizes the results from the dynamic simulation of the fuel management system with a single-speed, 40-W blower that is always kept on. The H_2 utilization on the UDDS and HWFET cycles is maintained at about 50% for >30% of the rated FCS power, but it is much less than 50% near idling conditions. With hydrogen feed rate being proportional to the pressure differential between anode and cathode inlets, H_2 utilization can be >60% during rapid deceleration that depressurizes the anode gas channels. Figure 2d also includes the calculated ejector pumping power defined as the flow rate of the entrained gas times the pressure head. We see that the pumping power can approach 400 W, which is equivalent to a 1-kWe reduction in parasitic power (i.e., power that a 40%-efficient blower would need to provide if the system did not include an ejector).

We ran simulations in which the feed hydrogen contains inert impurities at levels of 100-ppm N_2 and 200-ppm He [5]. The simulations include crossover of N_2 from cathode to anode and the crossover of He from anode to cathode. We determined the dynamic buildup of the inerts assuming that 15 standard liters of anode gas (equivalent to 2 times the volume of the anode circuit) are purged by supplying H_2 at the maximum flow rate (150% of the H_2 flow rate at rated power) when the inerts build up to 10 mol%. Our simulations indicate that the purge schedule is largely determined by the crossover of N_2 from cathode air rather than the level of impurities in feed hydrogen.

We determined the purge loss and the interval between purges for constant FCS power and on UDDS and HWFET drive cycles. We found that H_2 purge loss increases as the FCS power decreases; it can exceed 10% of the feed near idling conditions. Also, the purge schedule and loss are proportional to the allowable N_2 concentration in the anode channels. Thus, the interval between purges will be nearly twice as long, and the purge loss will be nearly half as much, if the allowable N_2 concentration is increased from 10% to 20%.

Performance of the Water Management Subsystem

For the membrane humidifier for the cathode inlet air, we developed a transient model to determine the heat and mass transfer between the counterflowing wet and dry streams that are separated by a perfluorosulfonic acid (PFSA) membrane [6]. The model considers water uptake from the wet stream, diffusion through the PFSA membrane, and desorption into the dry stream. The model was validated against experimental data from a full-scale (appropriate for an 80-kW_e automotive FCS), a half-scale, and a sub-scale ($1/10^{th}$) unit assembled as a bundle of Nafion® tubes arranged like a shell and tube heat exchanger [6].

We used the model to analyze the performance of a planar humidifier (20-μm-thick membrane, 3 m^2 active area) sized to raise the dew point temperature of cathode air (S2 configuration) to 61°C by transferring moisture from the spent saturated air leaving the stack at 75°C. The dry air temperature is lowered from 120°C at compressor discharge to 65°C in a pre-cooler.

Figure 3a shows the modeled performance of the humidifier on UDDS and HWFET cycles. The results are shown as a scatter plot of cathode air relative humidity (RH) calculated at the stack (bipolar plate) inlet temperature (nominally 65°C). The triangle symbols designate the results for the initial startup time when the stack and other components are still warming up. The square symbols represent results after the coolant temperature at stack inlet reaches 65°C. A >100% RH in Figure 3a implies that the cathode air is leaving the humidifier at a temperature higher than the bipolar plate temperature at stack inlet. Both

steady-state and dynamic simulations follow the general trend that the RH first increases as the air flow rate (FCS power) is reduced, reaches a peak, and then decreases as the CEM reaches the turndown limit. In the turndown limit, the cathode stoichiometry increases as the FCS power is reduced (see Figure 3a) and at certain points, the RH of air at the stack outlet may drop well below 100%.

Performance of the Thermal Management Subsystem

We analyzed the performance of a cross-flow automotive radiator with 40 plain microchannel fins per inch (0.4 m^2 frontal area, 2.3 m^2 fin area, 500 W blower fan) and evaluated its ability to reject the waste heat from an 80-kW_e S2 system [3,7]. We concluded that the fuel cell powertrains might need to be derated for ambient temperatures higher than 40°C since the fan power doubles for every 5°C increase in ambient temperature. We assessed the prospect of allowing stack temperatures to rise to 95°C under transient conditions (e.g., hill climbing at 55 mph) where high heat rejection may be required for several minutes. We determined that the maximum stack temperature is limited by the system pressure and the dew-point temperature of the cathode air at stack inlet. Also, under these conditions of high load, the CEM motor power may limit the ability to pressurize the cathode air adequately if the CEM does not include an expander.

We ran dynamic simulations of the heat rejection system on UDDS and HWFET cycles using a dynamic control strategy that operates at three levels. First, the flow rate of the stack coolant is varied linearly with the FCS power. Second, the thermostatic valve is completely open so that the coolant bypasses the HTC radiator if the stack outlet temperature is below a minimum set point (70°C). The valve is completely closed to allow all the coolant to flow through the radiator if the coolant temperature is above the design point (75°C). The bypass fraction is linearly varied between 0 and 1 if the coolant temperature is between the two set points. Third, the radiator fan is operated in on-off mode, i.e., the single-speed fan operates only if the coolant temperature at stack inlet exceeds 65°C.

Our results indicate that it takes about 500 s for the polymer electrolyte membrane fuel cell (PEMFC) stack and the stack coolant to reach their design temperatures on the UDDS cycle with cold start from 300 K. After this time, the coolant temperature fluctuates due to variations in vehicle speed (i.e., flow rate of ram air), stack heat load, continuous adjustment of the thermostatic valve, and the blower fan turning on and off.

Stack and System Performance

A two-dimensional model [3] was adapted to analyze the performance of a stack with NSTFC-based membrane-electrode assemblies. The NSTFC-specific constants for the model were derived from experimental data with 25-cm^2 active area cells [8].

Figure 4a presents the polarization curves constructed from the results for cold-start simulation on UDDS and HWFET cycles and for steady-state operation (system S2). The operating pressures in these simulations varied with current density (air flow rates) as determined by the CEM module. The scatter in cell voltage for the same current density is due to variations in stack temperature over time, cathode stoichiometry (higher during deceleration), and cathode inlet pressure (function of flow rate and shaft rpm). We have identified the coolant exit temperatures for some of the data points in Figure 4a to indicate the dominating effect of stack temperature on the polarization curves. The results indicated that flooding limits the stack power to ~32 kW_e at 30°C and ~50 kW_e at 45°C.

Figure 3b presents the relative humidity of the anode stream at the inlet to the stack. Since there is no humidifier in the anode circuit, and the feed H_2 is dry, the

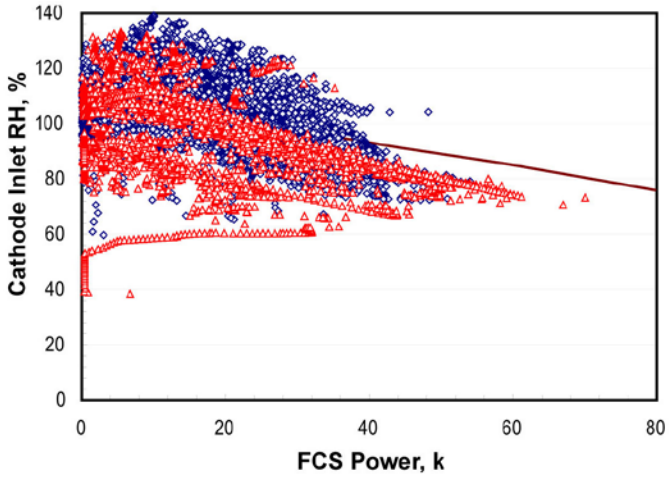

a) Inlet Cathode RH

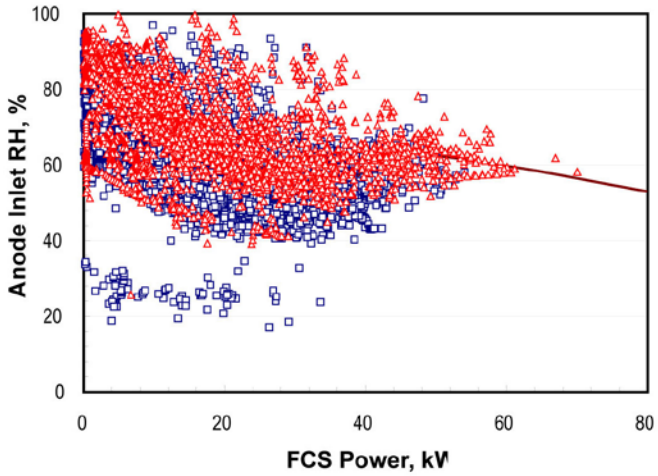

b) Inlet Anode RH

(symbols: dynamic results; solid line: steady-state simulation)

FIGURE 3. Dynamic Performance of the Water Management Subsystem

humidification of the anode stream is entirely due to water transport from the cathode through the membrane and recycle of the spent anode gas. As in Figure 3a, the triangle symbols designate the results for the initial startup time when the stack and other components are still warming up, and the square symbols represent results after the coolant temperature at stack inlet reaches 65°C. The isolated points with very low humidities represent instances of time that the anode is purged to relieve N_2 buildup and the accompanying loss of moisture with the purge gas.

Finally, Figures 4b and 4c summarize the instantaneous FCS efficiency on the UDDS and HWFET drive cycles. We see a larger spread in the efficiencies if the CEM motor is operated as motor/generator. The sporadic high efficiency points in the CEM generator (CEMG) mode are due to power generated by the air management system during rapid deceleration. These are generally followed by sporadic low efficiency points because of the parasitic power consumed in spinning-up of the CEMG shaft to higher speeds.

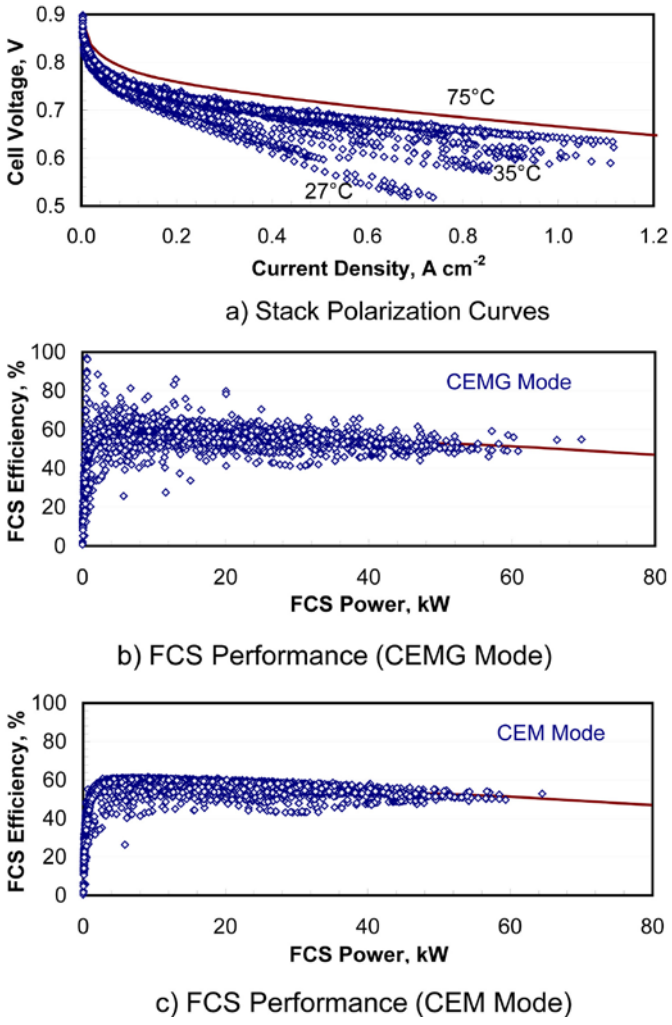

(symbols: dynamic results; solid line: steady-state simulation)

FIGURE 4. Dynamic Performance of the PEFC Stack and FCS on UDDS and HWFET Cycles

Conclusions and Future Directions

- System performance and stack polarization curves can deviate significantly from the steady-state values, especially during startup from 300 K. The transient FCS efficiency can be much higher than the peak steady-state efficiency during deceleration, or much lower during acceleration and while the stack is below its normal operating temperature of 75°C.
- Operating the CEM motor as motor/generator improves the CEM response during deceleration, although the transient cathode stoichiometry can still be >2 (design point stoichiometry ratio) at low loads and >>2 in the CEM's turndown limit.
- A hybrid blower-ejector arrangement controlled by a differential pressure sensor can maintain H_2 utilization at 50% or lower on the UDDS and HWFET drive cycles. A periodic purge is needed to control the buildup of N_2 in the anode recycle loop due to crossover from cathode air.
- At low loads, the RH can exceed 100% at cathode inlet (60% at design rated power) and reach 80-90% at the anode inlet (50% at design rated power), even without an external anode humidifier.
- In FY 2012, we will investigate the effects of alternative system configurations, rated power efficiency (Pt content) and system operating points on the high-volume manufacturing cost, dynamic drive-cycle performance, and component durability.

FY 2011 Publications/Presentations

1. R.K. Ahluwalia , X. Wang, J. Kwon, A. Rousseau, J. Kalinoski, B. James, and J. Marcinkoski, "Performance and Cost of Automotive Fuel Cell Systems with Ultra-low Platinum Loadings," *J. Power Sources*, 196 (2011), 4619-4630.

2. D. Myers, X.-P. Wang, R. Ahluwalia, X. Wang, M. Smith, and J. Gilbert, "Degradation Mechanisms of Pt-based Oxygen Reduction Reaction Electrocatalysts," 2010 Gordon Research Conference on Fuel Cells, Bryant University, Smithfield, RI, August 1–6, 2010.

3. R.K. Ahluwalia, X. Wang, R. Kumar, J. Kwon, and A. Rousseau, "Fuel Cell Systems with Low-Pt Loading: Cost vs. Performance," Fuel Cell Technical Team Meeting USCAR, Southfield, MI, August 18, 2010.

4. X. Wang and R.K. Ahluwalia, "Water Management in Polymer Electrolyte Fuel Cells," 218th ECS Meeting, Las Vegas, NV, October 10–15, 2010.

5. R.K. Ahluwalia, X. Wang, J. Kwon, A. Rousseau, J. Marcinkoski, and N. Garland, "Performance of Automotive Fuel Cell Systems with Ultra-low Platinum Loadings," 2010 Fuel Cell Seminar & Exposition, San Antonio, TX, October 18–22, 2010.

6. R.K. Ahluwalia , "Fuel Cells for Transportation: Status, Challenges and Prospects," Invited Presentation, Graduate Seminar Series, Department of Mechanical Engineering-Engineering Mechanics, December 2, 2010, Michigan Technological University, Houghton, MI.

References

1. R.K. Ahluwalia, X. Wang, K. Tajiri, and R. Kumar, "Fuel Cell Systems Analysis," 2010 DOE Hydrogen Program Review, Washington DC, June 8–11, 2010.

2. M.K. Gee, "Cost and Performance Enhancement for a PEM Fuel Cell System Turbocompressor," FY 2005 Annual Progress Report, DOE Hydrogen Program, 985, 2005.

3. R.K. Ahluwalia, X. Wang, J. Kwon, A. Rousseau, J. Kalinoski, B. James, and J. Marcinkoski, "Performance and Cost of Automotive Fuel Cell Systems with Ultra-Low Platinum Loadings," *J. Power Sources*, 196, 4619, 2011.

4. R.K. Ahluwalia and X. Wang, "Fuel Cell Systems for Transportation: Status and Trends," *J. Power Sources*, 177, 167, 2008.

5. H. Tomioka, "Prospect of ISO14687-2," ISO/TC192/WG12 Meeting, Vancouver, BC, 2009.

6. X. Wang and R. Ahluwalia, "Water Management in Polymer Electrolyte Fuel Cells," 218th ECS Meeting, Las Vegas, NV, October 2010.

7. Z. Mirza, "Development of Thermal and Water Management System for PEM Fuel Cell," 2010 DOE Hydrogen Program Review, Washington DC, June 8–11, 2010.

8. M.K. Debe, "Advanced Cathode Catalysts and Supports for PEM Fuel Cells," Grant No. DE-FG36-07GO17007, FreedomCAR Technical Team Review, Detroit, MI, March 10, 2010.